J|A|C|S
ARTICLES
Published on Web 08/26/2004

In Silico Assembly of Alzheimer's Aβ_{16-22} Peptide into β-Sheets

Sébastien Santini,[†] Normand Mousseau,[‡] and Philippe Derreumaux*[,§]

Contribution from the Information Génomique et Structurale, UPR 2589 CNRS, 31 Chemin Joseph Aiguier, 13402 Marseille Cedex 20, France; Département de physique and Regroupement québécois sur les matériaux de pointe, Université de Montréal, C.P. 6128, succ. center-ville, Montréal (Québec), Canada; and Laboratoire de Biochimie Théorique, UPR 9080 CNRS, Institut de Biologie Physico-Chimique, 13 rue Pierre et Marie Curie, et Université Paris 7 Denis-Diderot, 75005 Paris, France

Received May 10, 2004; E-mail: Philippe.Derreumaux@ibpc.fr

Abstract: Recent studies suggest that soluble oligomers of amyloid-forming peptides have toxic effects in cell cultures. In this study, the folding of three Alzheimer's A β_{16-22} peptides have been simulated with the activation−relaxation technique and a generic energy model. Starting from randomly chosen states, the predicted lowest energy structure superposes within 1 Å rms deviation from its conformation within the fibrils. This antiparallel structure is found to be in equilibrium with several out-of-register antiparallel β-sheets and mixed parallel−antiparallel β-sheets, indicating that full structural order in the fibrils requires larger aggregates. Folding involves the formation of dimers followed by the addition of a monomer and proceeds through a generalized mechanism between disordered and native alignments of β-strands.

I. Introduction

Alzheimer's disease is characterized by the deposition of amyloid fibrils sharing a common cross β-sheet structure with β-strands perpendicular to the fiber axis and β-sheets propagating along the direction of the fiber.[1,2] One of the major components of the plaques is a small peptide known as amyloid-β (Aβ) peptide with 40 (A β_{1-40}) or 42 (A β_{1-42}) amino acids, which is produced through endoproteolysis of the amyloid β protein precursor, a type I integral membrane protein.[3] It is believed that polypeptide aggregation proceeds through the formation of transient (thermodynamically unstable) intermediates which assemble into more stable oligomers (paranuclei). Once these paranuclei are formed, the growth of protofibrils is rapid, followed, eventually, by a maturation into amyloid fibrils.[4] Surprisingly, recent in vitro and in vivo studies indicate that both soluble β oligomers and insoluble Aβ fibrils are cytotoxic.[5] Since such soluble aggregates may also be involved in other neurodegenerative diseases[6−8] and apparently share a unique common structural feature, independently of the amino acid compositions,[9] it is important to understand at an atomic level the mechanisms responsible for Aβ peptide assembly. These efforts could lead to a more efficient design of new inhibitors.

It has been suggested, using circular dichroism spectroscopy and electron microscopy, that intermediate oligomeric states with α-helix character could be key intermediates in fibril assembly of several Aβ_{1-42} and Aβ_{1-40} variants.[10−12] Other studies, using gel electrophoresis, size exclusion chromatography, light scattering, and photoinduced cross-linking of unmodified proteins, indicate that the size of the nucleus is system-dependent within the nucleation-growth kinetic model.[13,14] Polymerization starts with the formation of pentamer/hexamer units (paranuclei) for Aβ_{1-42},[14] whereas the oligomer size distribution is a mixture of monomers, dimers, trimers, and tetramers in rapid equilibrium for Aβ_{1-40}[10] and of dimers and tetramers in rapid equilibrium for Aβ_{14-23}.[15]

Several simulations of amyloidogenic peptides have been reported. Nussinov and collaborators studied possible multilayer β-sheet oligomer organizations of several peptides by high-temperature molecular dynamics (MD) simulations in explicit water. These peptides include the Alzheimer's fragments Aβ_{16-22}, Aβ_{16-35}, and Aβ_{10-35},[16] the NFGAIL peptide derived from the human islet amyloid protein[17] and the 113−120

[†] Information Génomique et Structurale.
[‡] Université de Montréal.
[§] et Université Paris 7 Denis-Diderot.

(1) Serpell, L. *Biochim. Biophys. Acta* **2000**, *1502*, 16−30.
(2) Stefani, M.; Dobson, C. *J. Mol. Med.* **2003**, *81*, 678−99.
(3) Selkoe, D. *Trends Cell. Biol.* **1998**, *8*, 447−53.
(4) Jarrett, J.; Lansbury, P., Jr. *Cell* **1993**, *73*, 1055−8.
(5) Walsh, D.; Klyubin, I.; Fadeeva, J.; Cullen, W.; Anwyl, R.; Wolfe, M.; Rowan, M.; Selkoe, D. *Nature* **2002**, *416*, 535−9.
(6) Scherzinger, E.; Lurz, R.; Turmaine, M.; Mangiarini, L.; Hollenbach, B.; Hasenbank, R.; Bates, G.; Davies, S.; Lehrach, H.; Wanker, E. *Cell* **1997**, *90*, 549−58.
(7) Conway, K.; Lee, S.; Rochet, J.; Ding, T.; Williamson, R.; Lansbury, P., Jr. *Proc. Natl. Acad. Sci. U.S.A.* **2000**, *97*, 571−6.
(8) Narayanan, S.; Bosl, B.; Walter, S.; Reif, B. *Proc. Natl. Acad. Sci. U.S.A.* **2003**, *100*, 9286−91.
(9) Kayed, R.; Head, E.; Thompson, J.; McIntire, T.; Milton, S.; Cotman, C.; Glabe, C. *Science* **2003**, *300*, 486−9.
(10) Bitan, G.; Vollers, S.; Teplow, D. *J. Biol. Chem.* **2003**, *278*, 34882−9.
(11) Kirkitadze, M.; Condron, M.; Teplow, D. *J. Mol. Biol.* **2001**, *312*, 1103−19.
(12) Fezoui, Y.; Teplow, D. *J. Biol. Chem.* **2002**, *277*, 36948−54.
(13) Levine, H., III. *Neurobiol. Aging* **1995**, *16*, 755−64.
(14) Bitan, G.; Lomakin, A.; Teplow, D. *J. Biol. Chem.* **2001**, *276*, 35176−84.
(15) Tjernberg, L.; Callaway, D.; Tjernberg, A.; Hahne, S.; Lilliehook, C.; Terenius, L.; Thyberg, J.; Nordstedt, C. *J. Biol. Chem.* **1999**, *274*, 12619−25.
(16) Ma, B.; Nussinov, R. *Proc. Natl. Acad. Sci. U.S.A.* **2002**, *99*, 14126−31.

fragment of Syrian hamster prion protein.[18] Tiana et al. extended further this approach by calculating the free energies of dimers, tetramers, and octamers of the Aβ_{12-28} peptide.[19] These studies provide energetic insights into different arrangements but do not explain the assembly process.

Harrison et al.[20] and Dima and Thirumalai[21] explored protein aggregation and self-propagation using Monte Carlo simulations of lattice protein models. They found that chain polymerization is consistent with template assembly, with the dimer being the minimal nucleus. Gsponer et al. simulated the dynamics of the heptapeptide GNNQQNY from the yeast protein prion into trimers using the CHARMM force field and a solvent-accessible surface model.[22] They found that the preferred pathway for a trimer packed in a parallel β-sheet conformation is not associated to a downhill free energy profile because of the existence of mixed parallel−antiparallel β-sheets and parallel β-sheets with different hydrogen bond (H-bond) patterns. Finally, two folding simulations on Aβ_{16-22} have yielded conflicting results on the nature of the intermediates. Obligatory α-helix intermediates were found by all-atom MD simulations on the trimer in explicit solvent.[23] However, the criteria used for assigning the secondary structural elements within the MD-generated structures were not standard, and the simulations used a bias to facilitate interactions between the peptides. In contrast, our work on a dimer, based on the activation−relaxation technique (ART) and the generic OPEP (Optimized Potential for Efficient peptide-structure Prediction) energy model, showed that there are multiple folding pathways for dimer formation but that intermediates containing 30% α-helix are not obligatory.[24,25]

In this study, we perform ART−OPEP folding simulations of the trimer of Aβ_{16-22}, Ac−KLVFFAE−NH_2 (i.e., blocked with acetyl and amide groups as done experimentally[26]) as described in previous reports.[24,25] We recognize that the residues 30−35 and the length of the C- and N-termini are important kinetic determinants for Aβ peptides polymerization.[10,27,28] Nonetheless, Aβ_{16-22} is one of the shortest fibril-forming β-amyloid fragments yet reported[26] and thus an ideal probe for understanding the early steps of aggregation at an atomic level by computer simulations. Furthermore, almost all occurring Alzheimer's disease-causing mutations in Aβ_{1-40} cover the region 16−22, namely A21G, E22Q, E22K, E22G, and D23N; and several peptides derived from this region, e.g., KLVFF[29] and LPFFD,[30,31] block amyloid fibril formation in vitro.

II. Materials and Methods

ART−OPEP Simulations. For each chain, all backbone atoms are included and all side chains are modeled by a bead.[32,33] The OPEP energy model (version 1.3), which includes solvent effects implicitly, is expressed as a function of three types of interactions: excluded-volume potential between all particles and quadratic potentials for maintaining stereochemistry (bond lengths and bond angles connecting all particles and improper dihedral angles of the side chains with respect to the backbone), contact potential between side chains represented by a 12−6 potential if the interactions are hydrophobic in character and by a 6-potential, otherwise, and backbone two-body and four-body (cooperative) hydrogen bonding interactions.[24,32] This generic force field, optimized on the structures of short monomeric peptides but not Aβ, has been used in ART or another Monte Carlo-based method to predicting the native structures of small proteins adopting a wide range of topologies in solution.[25,33−35] These topologies include β-hairpin,[32,36] three-helix bundle,[33] and two β-hairpins packed against a helix,[37] among others.

ART is designed to explore efficiently the space of conformations while producing a physical trajectory composed of fully connected local minima separated by first-order saddle points; such a trajectory cannot be obtained by methods such as multiple tempering, for example.[25] ART focuses on the activated events which bring the protein from one conformation to another, ignoring the time spent by the protein as it vibrates thermally around a metastable minimum.[38,39] As a result, ART generates with the same efficiency simple or complex moves with low or high energy barriers. A basic ART event consists of four steps:[34] starting from a minimum, the system is first distorted along a direction taken at random in the 3N-dimensional space. The distortion is slowly increased until the lowest eigenvalue in the Hessian matrix representing the curvature of the energy landscape becomes negative. The system is then pushed along the eigenvector associated with the negative eigenvalue, while the energy is minimized in the hyperplane perpendicular to this direction until the total force on all atoms vanishes, indicating the convergence to a first-order saddle point. Subsequently, the system is pushed slightly over the saddle point and is relaxed (minimized) to a new minimum. Finally, the newly generated configuration is accepted/rejected using the Metropolis criterion.[40] All ART simulations presented here were conducted at $T_{\text{Metropolis}} = 600$ K for 12 000 events. Since ART only considers conformations in their local-energy minima, the $T_{\text{Metropolis}}$ does not correspond to a real thermal bath, and the effective temperature is therefore significantly lower than this number. Furthermore, we have shown on a 26-residue peptide model that ART trajectories are very similar at $T_{\text{Metropolis}}$ set to 300 and 600 K, but the use of high temperature reduces the chance of being trapped in a local minimum within the alloted number of ART events.[34]

The impact of the details of the OPEP force field on the ART trajectories and energy barriers crossed has been discussed elsewhere.[25,35] Despite limitations in OPEP (side chains are represented by sites and solvent is treated implicitly), previous tests on a helix model and a β-hairpin model have shown that the ART−OPEP trajectories follow closely those obtained by all-atom folding and unfolding simulations using more complex and physically based energy models with explicit solvent, although no previous method had managed to

(17) Zanuy, D.; Ma, B.; Nussinov, R. *Biophys. J.* **2003**, *84*, 1884−94.
(18) Ma, B.; Nussinov, R. *Protein Sci.* **2002**, *11*, 2335−50.
(19) Tiana, G.; Simona, F.; Broglia, R.; Colombo, G. *J. Chem. Phys.* **2004**, *120*, 8307−17.
(20) Harrison, P.; Chan, H.; Prusiner, S.; Cohen, F. *Protein Sci.* **2001**, *10*, 819−35.
(21) Dima, R.; Thirumalai, D. *Protein Sci.* **2002**, *11*, 1036−49.
(22) Gsponer, J.; Haberthur, U.; Caflisch, A. *Proc. Natl. Acad. Sci. U.S.A.* **2003**, *100*, 5154−9.
(23) Klimov, D.; Thirumalai, D. *Structure (Camb)* **2003**, *11*, 295−307.
(24) Santini, S.; Wei, G.; Mousseau, N.; Derreumaux, P. *Internet Electron. J. Mol. Des.* **2003**, *2*, 564−77.
(25) Santini, S.; Wei, G.; Mousseau, N.; Derreumaux, P. *Structure (Camb.)* **2004**, *12*, 1245−55.
(26) Balbach, J.; Ishii, Y.; Antzutkin, O.; Leapman, R.; Rizzo, N.; Dyda, F.; Reed, J.; Tycko, R. *Biochemistry* **2000**, *39*, 13748−59.
(27) Jarrett, J.; Berger, E.; Lansbury, P., Jr. *Biochemistry* **1993**, *32*, 4693−7.
(28) Liu, R.; McAllister, C.; Lyubchenko, Y.; Sierks, M. *J. Neurosci. Res.* **2004**, *75*, 162−71.
(29) Tjernberg, L.; Lilliehook, C.; Callaway, D.; Naslund, J.; Hahne, S.; Thyberg, J.; Terenius, L.; Nordstedt, C. *J. Biol. Chem.* **1997**, *272*, 12601−5.
(30) Soto, C.; Kindy, M.; Baumann, M.; Frangione, B. *Biochem. Biophys. Res. Commun.* **1996**, *226*, 672−80.
(31) Adessi, C.; Frossard, M.; Boissard, C.; Fraga, S.; Bieler, S.; Ruckle, T.; Vilbois, F.; Robinson, S.; Mutter, M.; Banks, W.; Soto, C. *J. Biol. Chem.* **2003**, *278*, 13905−11.
(32) Derreumaux, P. *J. Chem. Phys.* **1999**, *111*, 2301−10.
(33) Derreumaux, P. *Phys. Rev. Lett.* **2000**, *85*, 206−9.
(34) Wei, G.; Mousseau, N.; Derreumaux, P. *J. Chem. Phys.* **2002**, *117*, 11379−87.
(35) Wei, G.; Derreumaux, P.; Mousseau, N. *J. Chem. Phys.* **2003**, *119*, 6403−6.
(36) Wei, G.; Mousseau, N.; Derreumaux, P. *Proteins* **2004**, *56*, 464−74.
(37) Derreumaux, P. *J. Chem. Phys.* **2002**, *117*, 3499−503.
(38) Barkema, G.; Mousseau, N. *Phys. Rev. Lett.* **1996**, *77*, 4358−4361.
(39) Mousseau, N.; Derreumaux, P.; Barkema, G.; Malek, R. *J. Mol. Graphics Modell.* **2001**, *19*, 78−86.
(40) Metropolis, N.; Rosenbluth, A. W.; Rosenbluth, M. N.; Teller, A. H.; Teller, E. J. *J. Chem. Phys.* **1953**, *21*, 1087−92.

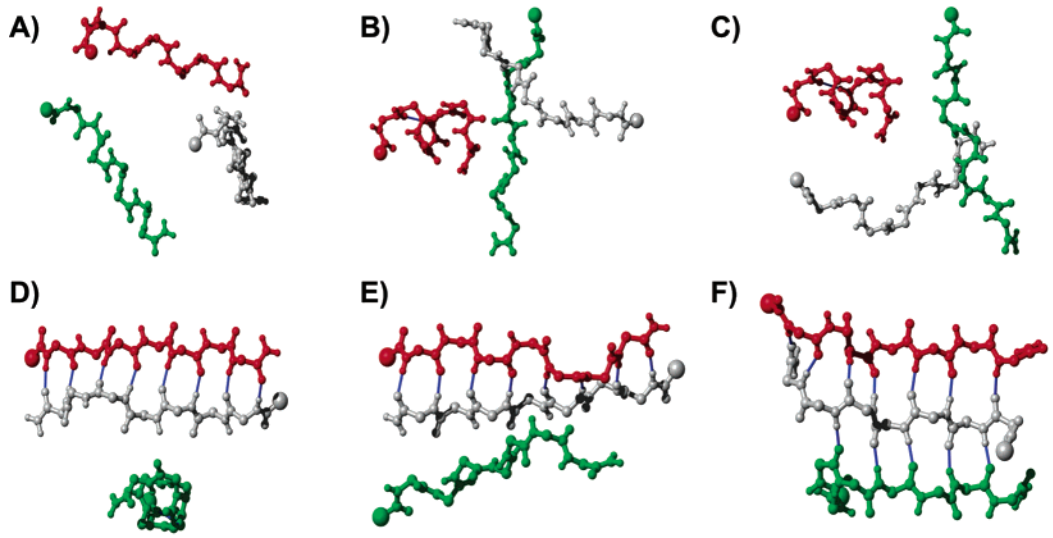

Figure 1. Initial structures for ART−OPEP simulations. The N-terminal end of each chain is located by a sphere. Figures were produced using the MOLMOL package.[50] The structure is used (A) in runs U3-1 to U3-5, (B and C) in runs U2H-1 to U2H-5, (D) in runs N2H-1 to N2H-5, (E) in runs N2U-1 to N2U-5, and (F) in the run N3. Here, the notation run X3-*i* or X2Y-*i* refers to the *i*th run where the number of chains X (3 or 2) are U (unfolded) or N (native) and the chain Y is U or H (α-helical).

detect all pathways.[34,36] The ART-generated trajectories provide therefore a detailed picture of possible assembly mechanisms.

In this work, we have selected to run 21 ART simulations starting from six distinct states and using different random-number seeds. The starting structures include three unfolded chains in randomly chosen orientations (Figure 1A), two unfolded chains and one α-helical chain (Figure 1B and C), an α-helix perpendicular to the native antiparallel β-sheet (Figure 1D), a disordered chain above the plane of the native antiparallel β-sheet (Figure 1E), and the native or NMR antiparallel β-sheets (Figure 1F). This ensemble of structures allows us to verify that the simulations locate the lowest-energy arrangements, independently of the initial orientations and conformations (random coil, α-helix and β-strand) of the chains, and to determine the differences in folding mechanisms with a dimer formed.

MD Simulations. Here, MD simulations were carried out to verify the stability of three ART-predicted conformations. These were performed in the canonical NPT (number of particles−pressure−temperature) ensemble at neutral pH for 20 ns using the program GROMACS and the energy function GROMOS96.[41] Each all-atom model was solvated in a dodecahedric box with a 40 Å side with ∼1400 SPC (simple point charge) water molecules and simulated using periodic boundary conditions. The temperature was kept close to 330 K, and the pressure, to 1 atm by weak couplings to external baths with standard constant times of 0.1 and 0.5 ps, respectively. This thermal bath corresponds to the experimental temperature often used to incubate amyloids. The SHAKE algorithm was used allowing an integration time step of 2 fs, and the Particle Mesh Ewald method was used with a cutoff distance of 12 Å for the electrostatics interactions.

III. Results and Discussion

In-Register vs Out-of-Register Antiparallel β-Sheets. In a recent report, we have shown that the peptide $A\beta_{16-22}$ is disordered and essentially a random coil in its monomeric form using OPEP and that the $A\beta_{16-22}$ dimer prefers an antiparallel orientation.[25] We also found that the assembly of a dimer can follow many paths, many of which involve a reptation of one monomer with respect to the other, a mechanism also seen for a β-hairpin, for example.[35] Here, we focus on the assembly process of a trimer, which allows us to identify, among others, the basic steps of oligomeric growth. Figures 2 and 3 show the predicted β-sheet registries and atomic models of the trimer by clustering the low energy conformations generated by all simulations using the C_α root-mean-square (rms) deviation and pattern of H-bonds. The secondary structure composition of each ART-generated frame was determined using the DSSP program.[42] All patterns of intermolecular H-bonds are compared to the NMR solid-state pattern of the fibril at pH 7.4:[26] an antiparallel β-sheet structure with a $16 + k \Leftrightarrow 22 - k$ β-sheet registry, i.e., intermolecular H-bonds between residues $16 + k$ and $22 - k$ of adjacent chains, with $k = 0$, 2, 4, and 6, and the C═O...HN and NH..O═C H-bonds formed.

Analysis of the results shows that 35% ($^7/_{20}$) of the runs locate three equienergetic antiparallel β-sheets with distinct registries of H-bonds. These β-sheets lie between −87 and −88 kcal/mol. The first alignment (A1), referred to as native, is the NMR solid-state antiparallel β-sheet structure with a $16 + k \Leftrightarrow 22 - k$ registry. The structures, obtained from the runs U2H-1 (two disordered chains and one chain helical) and N3 (the NMR solution), deviate by 1.2 Å rms from each other (Figure 2A). The second arrangement (A2) consists of a dimer in its native configuration with the third β-strand shifted by one residue in the NH2 direction from native alignment. This non-native register of H-bonds is attained in five runs starting either from three disordered chains (runs U3-1 and U3-2) or a helical chain perpendicular to a dimer (runs N2H-3, N2H-4, and N2H-5). The five predicted structures have a mean rms deviation of 1.6 Å (Figure 2B). The third arrangement (A3), obtained from two disordered chains and one helical chain (run U2H-2), ressembles the native one, except that the third β-strand is displaced by one residue in the acetyl direction with respect to native alignment (Figure 2C).

Since there is no experimental evidence that a three-chain A β_{16-22} system would be β-sheet-rich structured in solution, the three all-atom arrangements (A1-A3) were subject to 20-ns

(41) Berendsen, H.; van der Spoel, D.; van Drunen, R. *Comp. Phys. Commun.* **1995**, *91*, 43−56.

(42) Kabsch, W.; Sander, C. *Biopolymers* **1983**, *22*, 2577−637.

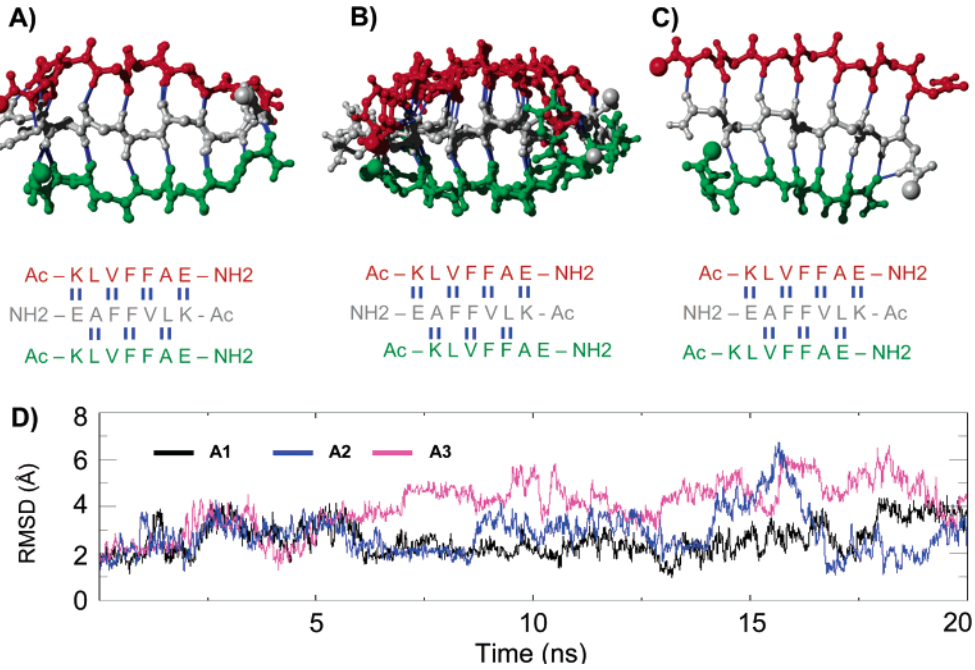

Figure 2. Lowest-energy β-sheet registries formed by Aβ16−22, as predicted by ART simulations. The hydrogen bonding interactions are in blue within the models and representated by double vertical bars in the registries. Structure A corresponds to the NMR pattern in the fibril (A1 arrangement), and structures B and C refer to the non-native A2 and A3 arrangements. The superposed structures in parts A and B result from independent runs, as indicated in the text. (D) The evolution of the RMS deviations (in Å) of the all-atom arrangements A1, A2, and A3 from their minimized structures by 20 ns MD simulations at 330 K in solution.

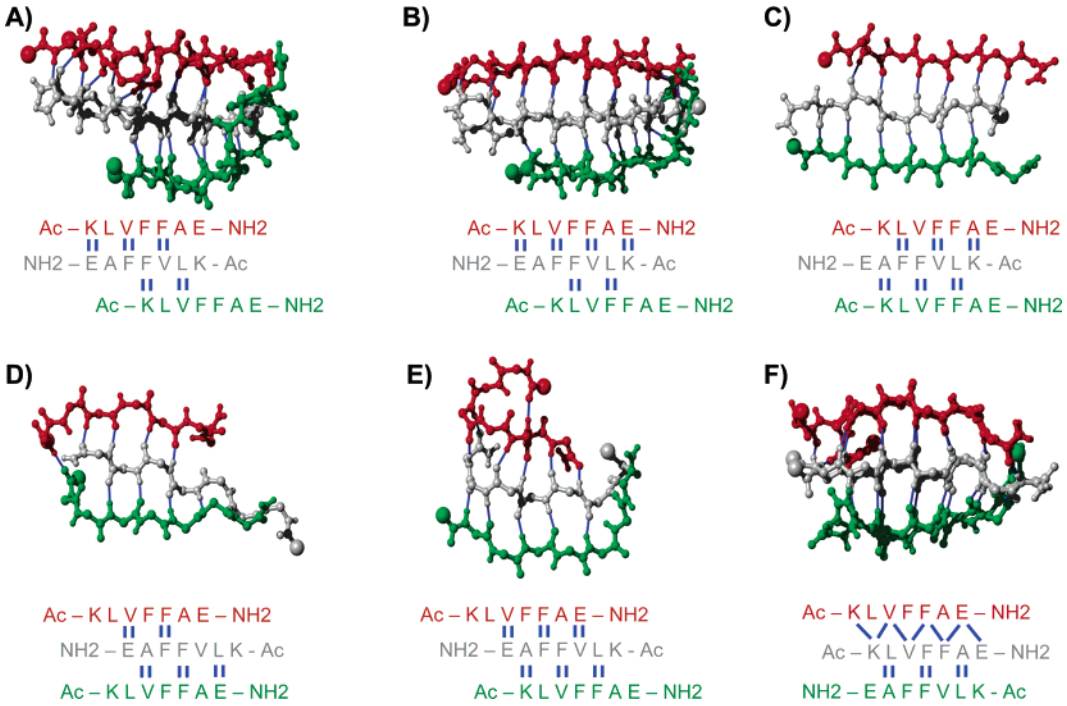

Figure 3. All-atom β-sheets of higher energies formed by Aβ16−22, as determined by ART simulations. Registries A to E are antiparallel in character, whereas registry F mixes parallel and antiparallel strands. The superposed structures in A, B, and F result from independent runs.

MD simulations at pH 7 and 330 K in explicit solvent. Figure 2D shows the C_α RMSD of the three models from their mimimized energy structures as a function of time. We see that the native (A1) and non-native (A2) alignments remain stable and behave similarly within the 20 ns time scale, although one strand may momentarily unfold in A2 (peak at 16 ns). In contrast, the model associated with the non-native A3 alignment shifts from a trimer to a dimer after 5.5 ns. We recognize that the time scale of these simulations is many orders of magnitude shorter than that in test tubes, but such a time scale is still beyond current computer facilities in explicit solvent. Taken together, these simulations covering 60 ns suggest that Aβ_{16-22} trimers are likely to be β-sheet ordered in solution at neutral pH.

The other 13 simulations evolve over 12 000 ART events into organized structures that do not correspond to one of the

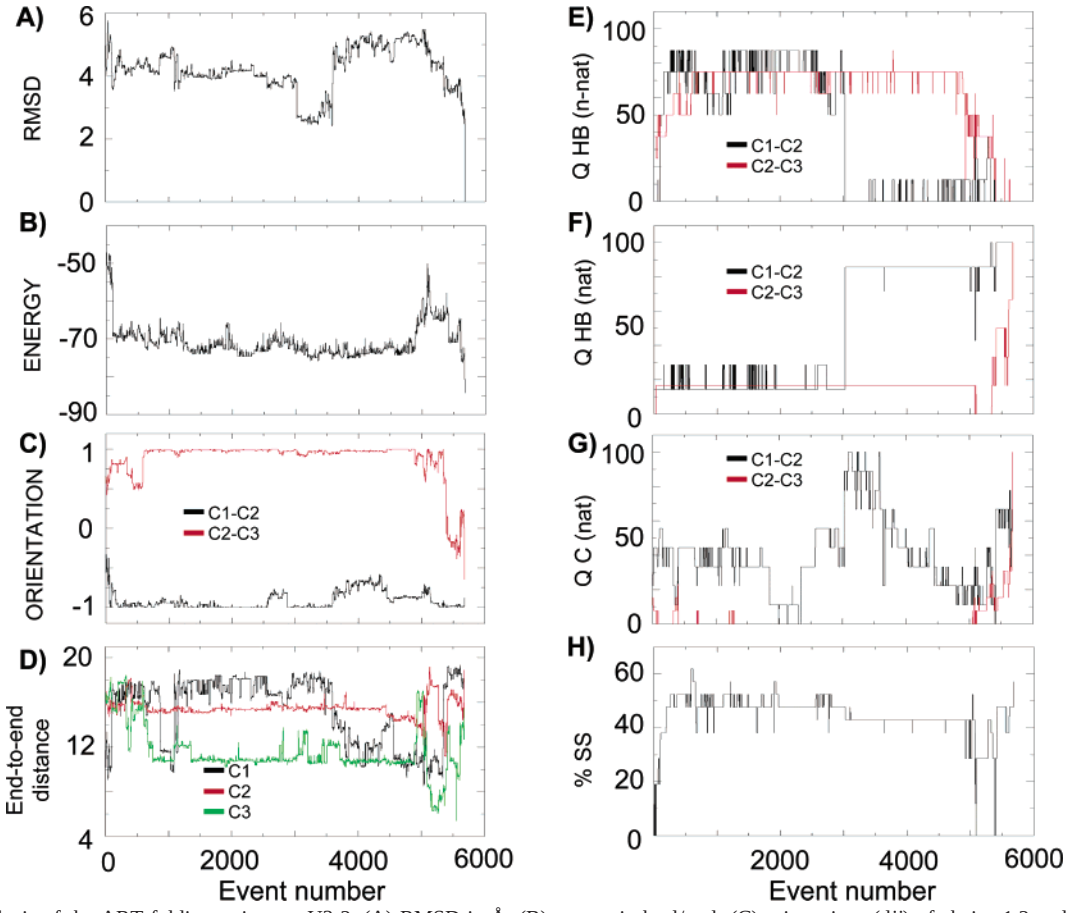

Figure 4. Analysis of the ART folding trajectory U3-2. (A) RMSD in Å; (B) energy in kcal/mol; (C) orientations (d*ij*) of chains 1,2 and chains 2,3; (D) end-to-end distances of the three chains in Å; percentage of non-native H-bonds (E) and native H-bonds (F) between chains 1 and 2 and between chains 2 and 3; (G) percentage of native contacts between the chains; and (H) percentage of secondary structures. For clarity, the results are given until the ground state is located. Only accepted events are shown.

three lowest-energy conformations. From tests, we know, however, that these runs would eventually reach the three equienergetic arrangements if they were continued.[35] These metastable conformations, lying between −79 (run U2H-5) and −85 (run U3−3) kcal/mol, consist of antiparallel β-sheets with out-of-register H-bond interactions, mixed parallel−antiparallel β-sheets, and unfolded conformations. The out-of-register antiparallel aggregates include one native dimer with the third β-strand partially formed and displaced by two or three residues (Figure 3A and B, runs N2U-4 and N2U-5), trimers where the central β-strand has been moved by one residue (Figure 3C, run N2H-2) or trimers where two β-strands were moved by several residues (Figure 3D-E, runs U2H-5 and U2H-4). The mixed β-sheets ($E = -85$ kcal/mol) include one parallel strand packed against two antiparallel in- (or out-of-) register strands (Figure 3F, runs U3-4 and U3-5).

Overall the energy surface we find, with low-energy in-register and out-of-register antiparallel β-sheets or mixed parallel−antiparallel β-sheets, ressembles that provided by recent MD analysis on a protein prion fragment, although the latter peptide prefers in-register parallel β-sheets.[22] These combined studies suggest that the energy gap among in-register, out-of-register, and mixed alignments is rather small, independently of the exact amino acid composition and that external conditions such as concentration, temperature, and pH can easily shift one β-sheet registry to another. This is consistent with NMR solid-state analyses. Petkova et al. showed that A β_{11-25} fibrils adopt antiparallel β-sheets with $17+k \Leftrightarrow 20-k$ registry at pH 7.4 vs $17+k \Leftrightarrow 22-k$ registry at pH 2.4.[43] Naito et al. found a pH-dependent antiparallel β-sheet registry in fibrils formed by the 32-residue human calcitonin, and that the fibril structure shifts from antiparallel β-sheets at pH 4.1 to a mixture of parallel and antiparallel β-sheets at pH 3.3.[44]

Several Folding Trajectories but One Unique Mechanism. The assembly process was monitored using several variables. These are the total energy E, the C_α rms deviation from the lowest energy arrangements, the scalar product (*dij*) between the end-to-end unit vectors of chains *i* and *j*, the end-to-end C_α distances of each chain (*DEi*), the percentages of native contacts (*QCij*) and native H-bonds (*QHBij*) between the chains, and the percentages of non-native H-bonds between the chains. Two side chains *k* and *l*, of van der Waals radii *Rk* and *Rl*,[32] are in native contact if they deviate by less than $Rk + Rl + 1$ Å from their positions in the native state. Since the 7-mer peptide contains LVFFA, *QC* follows essentially the formation of hydrophobic interactions. In what follows, chain 2 is the central strand within the native state.

Figure 4 offers a detailed description of the folding trajectory U3-2. Starting from disordered states (rms deviation 5 Å), chains 1 and 2 rapidly form an antiparallel β-sheet with non-native

(43) Petkova, A.; Buntkowsky, G.; Dyda, F.; Leapman, R.; Yau, W.; Tycko, R. *J. Mol. Biol.* **2004**, *335*, 247−60.
(44) Naito, A.; Kamihira, M.; Inoue, R.; Saito, H. *Magn. Reson. Chem.* **2004**, *42*, 247−257.

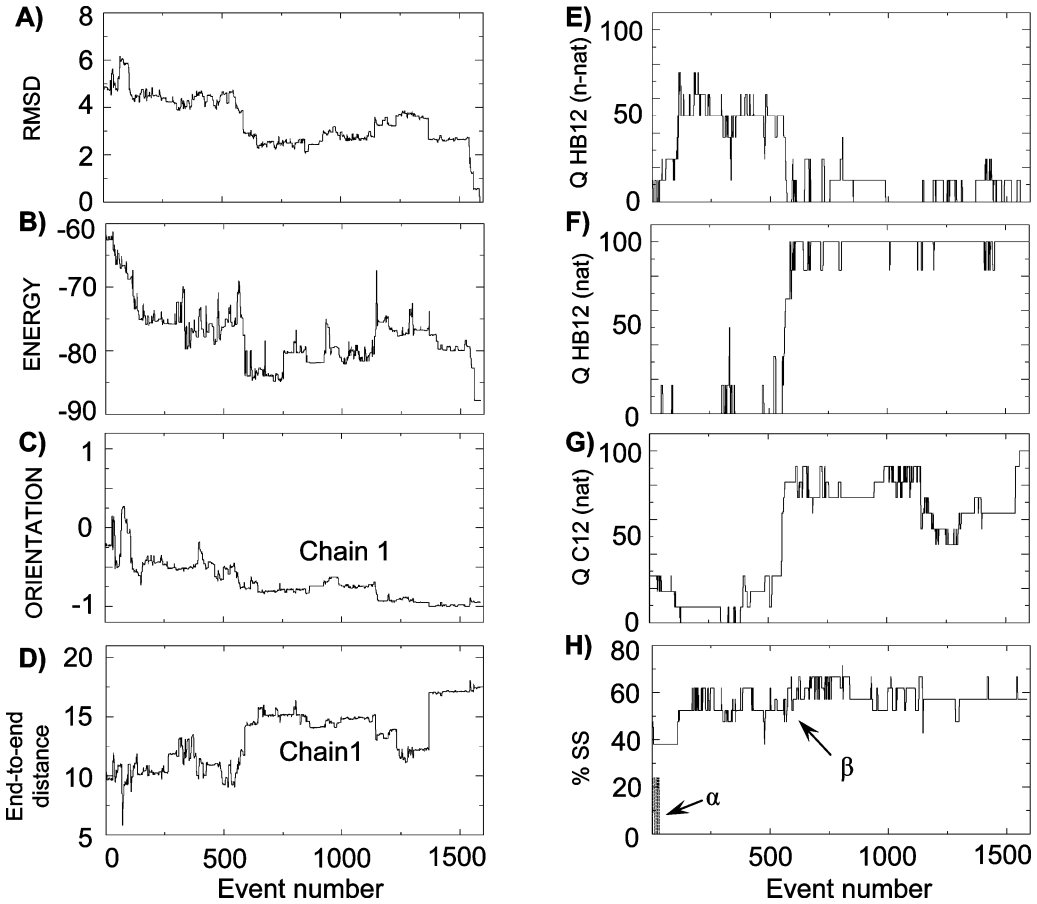

Figure 5. Analysis of the ART folding trajectory N2H-5. (A) RMSD in Å; (B) energy in kcal/mol; (C) orientation ($d12$) of chain 1 with respect to chain 2, (D) end-to-end distance of chain 1 ($DE1$) in Å; percentage non-native H-bonds (E) and native H-bonds (F) between chains 1 and 2; (G) percentage of native contacts between chains 1 and 2; and (H) percentage of secondary structures. For clarity, the results are given until the ground state is located, and the variables associated with chains 2 and 3 are not given because the dimer 23 is native throughout the run. Only accepted events are shown.

H-bonds (Figure 4E), whereas chains 2 and 3 are parallel for almost 5000 events ($d23 = 1$, Figure 4C). At event 2990, by a reptation move of one residue of strand 1 with respect to strand 2, dimer 12 adopts its native H-bond pattern (Figure 4E), $QC12$ and $QHB12$ increasing simultaneously to 80% and 100%, respectively (Figure 4F and G). From 3000 to 5000 events, the system remains within the same basin of attraction, and then chain 3 starts to rotate with respect to the dimer. Between events 5390 and 5619, $d23$ is 0, indicating a perpendicular arrangement of chains 2 and 3. This transition is made possible by the cooperative motion of the three chains, as deduced by the variation of the end-to-end C_α distances, and by the unfolding of chain 3 ($DE3 = 5.4$ Å at event 5551, Figure 4D). At that point, the trimer is still not fully formed: 1 native H-bond is formed within the dimer23 [between F20 of chain 2 and V18 of chain 3] and $QC23 = 20\%$. But, from there, the system rapidly propagates the H-bonds in both directions and reoptimizes simultaneously the interface within the dimer 12, as seen from the cooperative increase of all QC and QHB variables to their optimal values. Large variations in the assembly trajectories can occur using the same initial conformation and a different random-number seed. In run U3-1, the dimer 12 forms first as in run U3-2, but chain 3 goes directly to the antiparallel configuration. This facilitates convergence to the ground state, and the optimal antiparallel β-sheet is reached at event 639 vs 5674 in run U3-2.

Figure 5 reports the assembly process of run N2H-5 starting from a dimer of chains 2 and 3 with the remaining peptide in a helical conformation ($DE1 = 10$ Å, rmsd = 5.5 Å, $E = -62.6$ kcal/mol). Very similar results are obtained from N2H-3 and N2H-4. The helix rapidly relaxes to an unfolded state (event 32, Figure 5H) and within 500 steps, a non-native trimeric state is formed (Figure 5E). At event 500, chain 1 is neither fully extended ($DE1 = 9.3$ Å, Figure 5D) nor antiparallel with chain 2 ($d12 = -0.5$, Figure 5C) and makes four non-native H-bonds with the dimer. Then, at event 550, the reptation move of chain 1 breaks the four non-native H-bonds (Figure 5E) and form almost simultaneously the native pattern of H-bonds and side-chain contacts. As seen in Figure 5F and H, ($QHB12$, $QC12$) = (0, 20%) at event 555 vs (100%, 90%) at event 615. Finally, the system finds its ground state at event 1585.

Figure 6 shows some representative snapshots of the run U2H-1 starting from chain 3 helical and two chains disordered (Figure 6A). During the first 600 events, chain 3 remains helical (Figure 6F) and folding starts by the formation of dimer 12 with non-native β-sheet registry (Figure 6B). Between events 600 and 2500, chain 3 loses progressively its helical character and makes non-native hydrogen bonds with the dimer (Figure 6C). This non-native trimer is conserved until event 5530 where the reptation move of chain 3 allows the system to explore the arrangement A2 (Figure 6D). This conformation is retained between events 5530 and 11111, i.e., until the reptation move

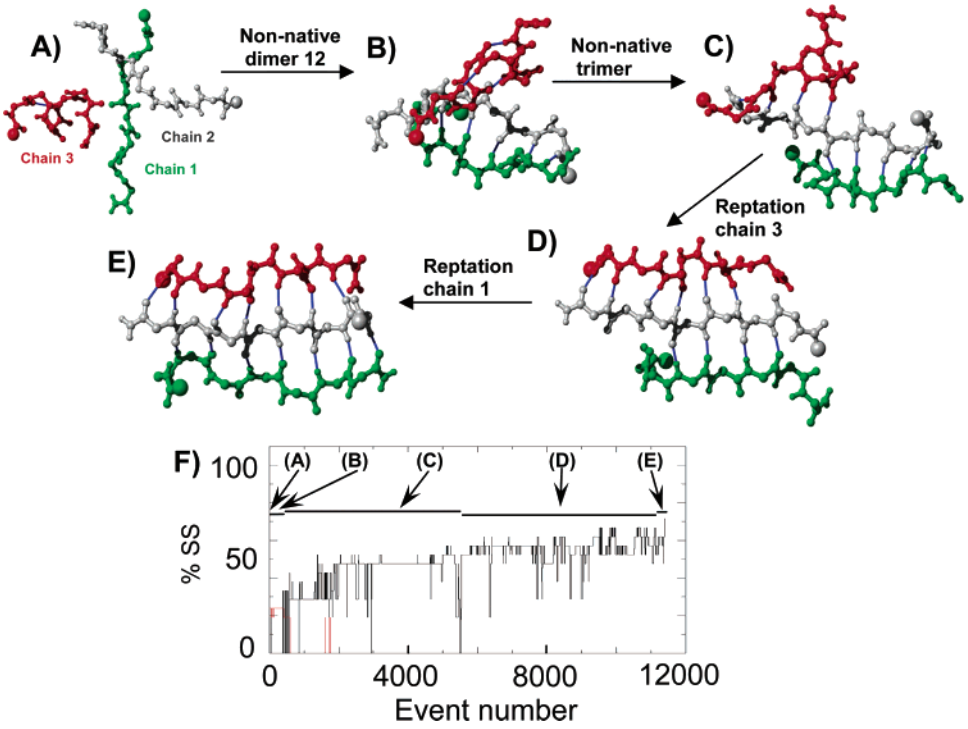

Figure 6. Representative snapshots of the ART folding trajectory U2H-1. (F) percentage of secondary structures as determined by DSSP42 as a function of accepted event numbers, with β-sheet in black and α-helix in red.

of chain 1 switches the trimer from the arrangements A2 to A1 (Figure 6E). The ground state is reached at event 11 398.

As expected from previous Monte Carlo simulations of lattice amyloid-forming protein models,[20,21] discontinuous MD simulations and Langevin dynamics simulations of multiple chains favoring the native state with a Go-energy model,[45,46] our unbiased simulations follow one unique mechanism described by monomers → dimers + monomer → trimers. In addition, the template reaction (N2 + U → N3) occurs on average more rapidly than the spontaneous reaction (U3 → N3). Within this mechanism, however, our ART simulations show that the folding routes involve non-native dimers during the U3 → N2 + U reaction and non-native trimers in the subsequent step. The exchange between non-native and native dimers is rather fast, on average within 2500 steps. We emphasize that even the 13 unfolded trajectories explore a native dimer. In contrast, the exchange between non-native and native trimeric alignments takes place rapidly in the folded trajectories but is not encountered in the unfolded trajectories within 12 000 events. This finding suggests that the reptation move of one strand with respect to the native dimer, i.e., the breaking of almost all-native H-bonds at once in order to form the native H-bond registry, is the rate-limiting step during the assembly process. The observation of this reptation mechanism in a three-chain system is not totally surprising. It is a fundamental movement in polymer chains and fluorescence microscopy shows that myosin can induce the reptation of actin filaments when adenosine triphosphate is added.[47] Interestingly, this motion has also been observed during the assembly of the prion fragment PrP109−122 in solution by isotope-edited infrared spectroscopy.[48]

Recently, it has been suggested by CD analysis that α-helical conformations could be key intermediates in fibril assembly of several $A\beta_{1-42}$ and $A\beta_{1-40}$ variants.[10−12] This feature has also been advocated by biased MD simulations simulations.[23] By following the secondary structure composition using the DSSP program,[42] we find that α-helical intermediates are encountered in the run U2H-1 (between 1550 and 1780 steps, as seen in Figure 6) but not in the other 5 folded trajectories and the 13 unfolded trajectories. This result raises questions regarding the role of these α-helical intermediates in $A\beta_{1-40}$. It remains possible that they are off-pathway, as it has been suggested for the soluble β-rich oligomers during the assembly process of prion proteins under destabilizing conditions.[49]

IV. Conclusions

Understanding the mechanism by which amyloid-forming peptides form protofibrils is an important step toward designing effective drugs. To address this issue, we have studied the folding assembly of three chains of the $A\beta_{16-22}$ peptide using ART−OPEP simulations. These are not biased toward specific structures and generate activated mechanisms responsible for the long-term dynamics of the system. Because of the approximations in the chain and solvent representations, we do not expect the present trajectories to reproduce exactly the experimental reality, which requires several days in test tubes. Nonetheless, our trajectories show several interesting features.

First, one stable structure for trimers is related to the experimentally determined structure for fibrils, but full structural order in fibril requires larger aggregates. We find that the three-

(45) Jang, H.; Hall, C.; Zhou, Y. *Protein Sci.* **2004**, *13*, 40−53.
(46) Friedel, M.; Shea, J.-E. *J. Chem. Phys.* **2004**, *120*, 5809−23.
(47) Humphrey, D.; Duggan, C.; Saha, D.; Smith, D.; Kas, J. *Nature* **2002**, *416*, 413−6.
(48) Silva, R.; Barber-Armstrong, W.; Decatur, S. *J. Am. Chem. Soc.* **2003**, *125*, 13674−5.
(49) Baskakov, I.; Legname, G.; Baldwin, M.; Prusiner, S.; Cohen, F. *J. Biol. Chem.* **2002**, *277*, 21140−8.
(50) Koradi, R.; Billeter, M.; Wuthrich, K. *J. Mol. Graphics* **1996**, *14*, 51−5.

chain system cannot distinguish between the fully in-register antiparallel β-sheet, as determined by NMR solid state, and out-of-register antiparallel β-sheets.

Second, the existence of various antiparallel β-sheets and antiparallel−parallel trimers help explain the observed dependency of β-sheet registries of several amyloidogenic peptides on pH conditions.[43,44] Furthermore, they are likely to provide an ideal pool of preaggregated material for larger oligomers and thus may facilitate the formation of a rich variety of protofibrils.

Finally, starting from various states, our simulations show that folding to an antiparallel trimer proceeds through one unique mechanism, although the details can vary from one trajectory to another. This assembly process, which takes place upon simultaneous optimization of the hydrophobic and hydrogen bonding interactions, involves the formation of dimers followed by the addition of a monomer. Further analysis reveals the existence of kinetically trapped alignments of β-strands during the folding process, which can be surmounted by the reptation move of one strand with respect to the others. The observation of this mechanism between disordered and native alignments is consistent with a recent isotope-edited IR spectroscopy study on a prion fragment[48] and might be a generalized process in the early steps of Aβ aggregation.

Acknowledgment. Sébastien Santini is supported by the *Natural Sciences and Engineering Research Council* of Canada. The ART calculations were done on the computers of the Réseau québécois de calcul de haute performance and the MD simulations at IGS, Marseille. N.M. is a Cottrell Scholar of Research Corporation.

JA047286I